HHS Public Access

Author manuscript

*J Control Release*. Author manuscript; available in PMC 2020 July 10.

Published in final edited form as:

*J Control Release*. 2019 July 10; 305: 29–40. doi:10.1016/j.jconrel.2019.05.022.

# Enhanced Anti-tumor Efficacy and Safety with Metronomic Intraperitoneal Chemotherapy for Metastatic Ovarian Cancer using Biodegradable Nanotextile Implants

**Smrithi Padmakumar**[1,2], **Neha N. Parayath**[1], **Shantikumar V Nair**[2], **Deepthy Menon**[2,3], and **Mansoor M. Amiji**[1,3]

[1]Department of Pharmaceutical Sciences, School of Pharmacy, Northeastern University, Boston, MA 02115 USA

[2]Centre for Nanosciences and Molecular Medicine, Amrita Institute of Medical Sciences, Amrita Vishwa Vidyapeetham, Kochi, Kerala, INDIA

## Abstract

The objective of this study was to evaluate intraperitoneal (IP) metronomic chemotherapy using sustained release paclitaxel (PTX) delivery from electrospun biodegradable polymeric yarns woven into suturable nanotextiles. Following confirmation of *in vitro* PTX efficacy in ID8-VEGF epithelial ovarian cancer cells, *in vivo* studies were performed upon surgical peritoneal implantation of nanotextile implants in orthotopic, syngeneic ID8-VEGF tumor-bearing C57BL/6 mice. In comparison to the clinical PTX-solution, there was a significant enhancement of anti-tumor efficacy and safety with PTX-nanotextiles. After 35-days, the peritoneum of tumor-bearing mice with PTX-nanotextiles was completely devoid of tumor nodules and ascitic fluid. Additionally, VEGF levels measured in peritoneal lavage fluid were 300-fold lower compared to PTX-solution and 600-fold lower as compared to untreated tumor-bearing animals. PTX-solution treated group also developed severe metastatic lesions and progressive ascitic fluid buildup. More importantly, no signs of systemic/ organ toxicity were observed in PTX-nanotextile implanted mice, unlike the systemic toxic effects induced by PTX-solution. Collectively, our results show the therapeutic and safety advantages offered by combining clinically translatable metronomic low-dose chemotherapy and IP pharmacokinetics using biodegradable nanotextile implants in addressing the challenges of late-stage ovarian cancer.

## Graphical Abstract

[3]Corresponding authors: Tel. (617) 373-3137, Fax (617) 373-8886, m.amiji@northeastern.edu; Tel. (91)484-6688750, Fax (91)484-2802030, deepthymenon@aims.amrita.edu.

**CONFLICT OF INTEREST:** The authors declare that they have no conflicts.

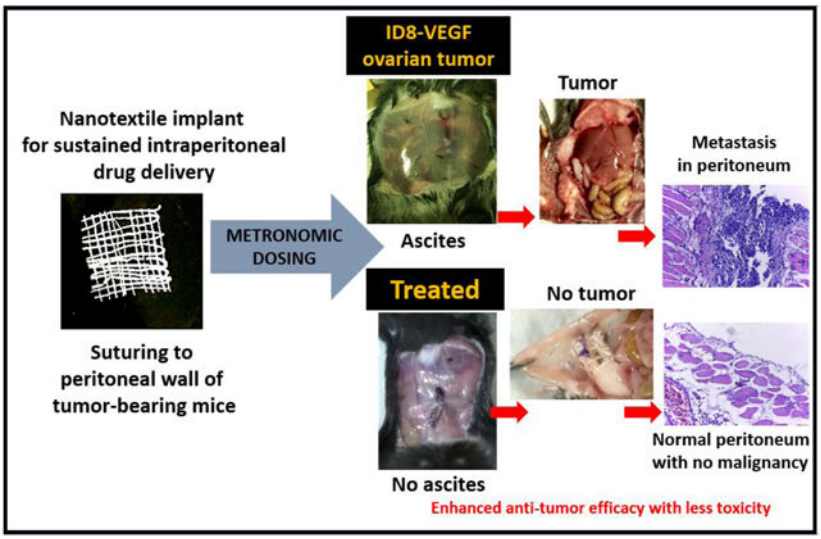


**Keywords**

Metronomic; intraperitoneal chemotherapy; paclitaxel; ID8-VEGF ovarian tumor model; biodegradable polymeric nanotextiles

## 1. INTRODUCTION

Ovarian cancer (OC) is the fifth leading cause of cancer-related deaths among women in the United States and one of the most common gynecological malignancies throughout the world [1]. According to the American Cancer Society statistics, 22,530 women will receive a new diagnosis of ovarian cancer and about 13,980 women will die from the disease in 2019 [2]. Additionally, the 5-year relative survival of OC patients is only 45% [3]. Patients are initially diagnosed by exploratory laparotomy, during which surgical staging is performed and gross disease is debulked. Unfortunately, most of the patients relapse and eventually die of disease within 12-18 months post-treatment [4,5]. Thus, despite aggressive surgery and chemotherapy, the chance of achieving long-term disease-free survival for subjects with stage III and stage IV disease is an abysmal 25% and <10%, respectively [6,7]. Although there is an initial high response rate to chemotherapy, disease relapse occurs in majority of cases due to accelerated tumor cell proliferation, lowered drug concentration at disease sites, and ultimately, resistance to maximum tolerated dose (MTD) chemotherapy [8-13]. Additionally, for an intravenously administered drug, an effective drug concentration is not available in the peritoneal cavity due to the presence of peritoneal-plasma barrier, thereby reducing the effect of intravenous (IV) chemotherapy on peritoneal metastases [14].

Since a majority of primary ovarian tumor as well as metastatic tumor progresses and remains within the peritoneal cavity, a drug delivery approach directed exclusively to the peritoneal cavity, such as intraperitoneal (IP) chemotherapy, could significantly improve the clinical outcome and patient survival [9,15]. Furthermore, intraperitoneal administration maximizes the total amount of drug delivered into residual peritoneal tumor nodules after debulking surgery. However, the clinical adoption of IP chemotherapy as a standard of care

is currently hampered by complications caused by indwelling intraperitoneal catheters and toxicity caused by bolus dosing regimens of drug solution [16].

An enhanced rate of tumor cell repopulation is reported to occur during the course of intermittent MTD chemotherapy cycles, which is administered conventionally with sequential drug-free breaks [9,17]. In this context, a localized and sustained IP drug delivery strategy that retains high drug concentrations within the peritoneal cavity, thereby avoiding treatment-free periods can substantially improve the patient-response to chemotherapy and reduce incidence of resistance development [18]. Furthermore, this would also mitigate the need for frequent drug dosing through IP injections/ indwelling catheters currently employed in clinics to address the issue of rapid drug clearance. Continuous IP dosing has been accomplished previously through drug depots in various forms such as particulate systems [19,20], although they were not able to render drug release profiles for prolonged durations. Injectable and implantable IP systems also posed severe issues with respect to shorter drug release periods, heterogenous drug distribution and migration to extraperitoneal regions [21-23]. Nevertheless, a low-dose metronomic regimen of continuous drug administration is established to provide significant anti-tumor and antimetastatic effects with less toxicity, through an anti-angiogenic mechanism [24,25]. Few studies have reported the preclinical and clinical benefits of metronomic therapy with oral/ peritoneal dosing of conventionally used chemotherapy drugs for effective treatment of ovarian cancer [26-29].

Hence, we hypothesized that a drug eluting intraperitoneal implant that releases the chemotherapy drug continuously in a sustained and metronomic manner can retain effective peritoneal drug concentrations, thereby improving therapeutic efficacy and safety. Our group has recently developed a suturable implant in the form of woven nanotextiles from electrospun polydioxanone (PDS) yarns incorporating paclitaxel (PTX) [30]. These yarn-based depots offered prolonged *in vivo* drug release profiles in a metronomic manner for >2 months in naive mice [30]. This was attributed to a a synergistic mechanism of drug diffusion and polymer degradation, coupled with the nanoarchitecture of fibrous yarn-based textiles. To elucidate the therapeutic utility of this metronomic PTX eluting nanotextile implant, it was surgically implanted in ID8-VEGF syngeneic orthotopic model of OC and investigated for a period of 35 days. The tumor responsiveness and safety were assessed relative to clinically used PTX-solution.

## 2. MATERIALS AND METHODS

### 2.1. Materials

Polydioxanone (PDS) (inherent viscosity 1.9 dL/g at 30 °C) was purchased from Evonik (Essen, North Rhine- Westphalia, Germany). Paclitaxel powder (molecular weight 853.91 Da) was procured from LKT Laboratories, St.Paul, MN, USA). 2,2,2-Trifluoroethanol for fabricating yarns was obtained from Acros Organics™ (Fair Lawn, NJ, USA). ID8-VEGF cells obtained from the University of Kansas (Kansas City, KS, USA) were cultured in RPMI-1640 (Sigma-Aldrich Co, St.Louis, MO, USA) supplemented with 10% fetal bovine serum (FBS) (HyClone, Logan, UT, USA), Antibiotic-antimycotic solution (Corning®-Mediatech Inc., Manassas, VA, USA), sodium pyruvate (Gibco®-Life Technologies, Carlsbad, CA, USA) and β-mercaptoethanol (MP Biomedicals, LLC, OH, USA) at 37 °C

and 5 % $CO_2$. Paclitaxel solution (PTX-solution) composition was constituted by dissolving 6 mg Paclitaxel (TSZ Chem, Framingham, MA, USA) in 1 mL of 50:50 (% v/v) Cremophor EL: ethanol mixture. Cremophor® EL was obtained from BASF (Mount Olive, NJ, USA) and absolute ethanol was purchased from Fisher Scientific (Fair Lawn, NJ, USA). 3-(4,5-dimethylthiazol-2-yl)-2,5-diphenyltetrazolium bromide (or MTT) reagent was procured from Sigma-Aldrich (St.Louis, MO, USA). Vicryl 4-0 and Monocryl 14-0 sutures were purchased from Ethicon (Johnson & Johnson, Bridgewater, NJ, USA). Potassium phosphate and orthophosphoric acid for HPLC mobile phase preparation were obtained from Fisher Scientific (Fair Lawn, NJ, USA) and Acros Organics™ (Fair Lawn, NJ, USA) respectively. Other HPLC-grade solvents, such as methanol and acetonitrile, ethyl acetate for PTX extraction and formalin for tissue fixation were purchased from Fisher Scientific (Fair Lawn, NJ, USA). Hematoxylin and eosin for H&E staining were purchased from Sigma-Aldrich (St.Louis, MO, USA). Antibodies Ki-67 and CD31 for Immunohistochemistry (IHC) analysis were procured from Abcam (Cambridge, MA, USA) and BioGenex (Fremont, CA, USA).

### 2.2. Fabrication of Woven Nanotextile Implants

PTX-loaded PDS yarns were fabricated by a modified electrospinning method previously reported by our group [31,32]. Briefly, PDS (15 % w/v) and paclitaxel (10 % w/w of PTX) were completely dissolved in 2,2,2-Trifluoroethanol (TFE) and the solution was used for electrospinning and nanofibrous yarn formation. Uniform and continuous yarns were obtained using previously optimized parameters [2 mL/h flow-rate, 12 kV voltage, 700 rpm collector-rotation and 0.5 m/min yarn-uptake rate] and they were subsequently air-dried inside a laminar flow hood at room temperature for 12 h. These yarns loaded with 10 % PTX were quantified to show an entrapment efficiency of 86 ± 10% by HPLC analysis [30]. They were further woven into loosely packed nanotextiles weighing ~ 20 mg using a plain weaving-loom (Little Weaver, AVL Looms, Chico, CA, USA).

### 2.3. *In Vitro* PTX Cytotoxicity Analysis in ID8-VEGF Cells

*In vitro* cytotoxicity of PTX from nanotextile and PTX-solution on VEGF expressing mouse ovarian surface epithelium (ID8-VEGF) cells was studied using the colorimetric MTT assay. The experimental strategy for assessing the cytotoxicity of PTX eluted from nanotextile implant was adapted from ISO protocol 10993:5- Extract test for biological evaluation of medical devices [33]. PTX released from the nanotextile into cell culture medium (RPMI, 37°C, 200 rpm shaking conditions) at different timepoints was evaluated by HPLC (Waters, Milford, MA, USA). The sample was injected into a 4.6×250 mm Qualisil gold 5 μm C-18 column kept at 30 °C, eluted with 80:20 of methanol: potassium dihydrogen orthophosphate buffer (pH 2.5 with $H_3PO_4$) at a flowrate of 0.5 mL/min. PTX was detected by a UV absorbance at 227 nm and at a retention time of 10.5 min. Having quantified the drug concentrations, these aliquots were further diluted with media to obtain equivalent concentrations as that of PTX-solution. ID8-VEGF cells at a seeding density of 8,000 cells per well in a 96-well microplate for 24 h were thereafter treated with PTX-solution and the released aliquots from nanotextiles, at concentrations ranging from 0.5 nM to 2.0 μM over 24, 28 and 72 h and percentage cell viability was assessed. The $IC_{50}$ values of PTX in aqueous solution and from nanotextiles were calculated.

### 2.4. Development of a Syngeneic Orthotopic ID8-VEGF OC Model

All animal studies were based on the protocol approved by Northeastern University's Institutional Animal Care and Use Committee (IACUC). Female C57BL/6 mice (4-6 weeks old, 20-25 g) purchased from Charles River Laboratories (Wilmington, MA, USA) were injected intraperitoneally with $4X10^6$ ID8-VEGF cells suspended in RPMI-1640 medium. The tumor inoculated animals were housed under controlled laboratory conditions and provided with free access to sterilized diet and drinking water. Animals were maintained on an automatic 12 h dark-fight cycle at 22-24 °C and monitored daily for body weight changes, abdominal circumference, food intake, fecal excretion, and mobility.

### 2.5. Treatment of Tumor-Bearing Mice with PTX in Solution and in Nanotextile Implant

The presence of tumor on day 8 post tumor inoculation was confirmed through quantification of peritoneal VEGF levels and Tumor Associated Macrophages (TAMs) in a previous study in ID8-VEGF syngeneic orthotopic ovarian tumor mice model [34]. Hence, day 8 post tumor inoculation was chosen as the timepoint for PTX treatment in this work and the tumor-bearing mice were evenly assigned to untreated group and groups treated with drug free (bare) nanotextile, PTX-solution and PTX-loaded nanotextile (n = 5 per group per time-point). The PTX dose for both solution and implant group was maintained constant at 20 mg/kg [29], which corresponds to the clinical human low-dose metronomic regimen of 60 mg/$m^2$ employed once every 3 weeks [5,35,36]. Animals of PTX-solution group were injected once with 20 mg/kg IP PTX-solution (PTX formulation in cremophor-ethanol solvent) and animals under PTX-nanotextile group were surgically implanted with nanotextile loaded with equivalent drug amount of 20 mg/kg. Woven nanotextiles (bare and PTX loaded) of 1×1 $cm^2$ (~15 mg) size were surgically implanted by suturing the implant along the peritoneal cavity wall of mice with Vicryl suture, after giving anesthesia with isollurane. The peritoneal incision was closed with Vicryl suture followed by skin closure with Monocryl suture. The control and test animals were observed daily for any changes in body weight and gradual abdominal distension indicating ascitic fluid accumulation. After 16, 24, and 35 days following tumor cell inoculation, five animals from each group were euthanized by $CO_2$ inhalation and asphyxiation. Thereafter, the mice peritoneal cavity was closely assessed for tumor nodules and ascites accumulation. Abdominal circumferences of mice were measured with a measuring tape, post day 27. Ascitic fluid/ peritoneal lavage collected at all timepoints was centrifuged at 400 xg for 7 min to segregate the cellular and acellular fractions. VEGF analysis was performed on the acellular fractions from the peritoneal lavage.

### 2.6. Assessment of *In Vivo* Drug Release by HPLC Analysis

The nanotextile implants explanted from mice upon euthanasia at timepoints of days 16, 24 and 35 were dissolved completely in TFE solvent. PTX was extracted and resuspended in HPLC mobile phase to quantify the remaining drug content in the implant at various timepoints. *In vivo* PTX-release from the nanotextile implant at each timepoint was calculated by subtracting the remaining drug amount at that timepoint from the initial drug content pre-implantation.

### 2.7. Measurement of VEGF Levels in IP Lavage Fluid by ELISA

Quantikine® ELISA mouse VEGF immunoassay kit (R&D systems, Minneapolis, MN, USA) was used to quantify VEGF levels in peritoneal lavage/ ascites samples by a quantitative sandwich enzyme immunoassay technique according to the manufacturer's instructions. Briefly, the lavage samples were incubated in pre-coated 96-well plate consisting of immobilized antibody specific for mouse VEGF for 2 h at room temperature. After washing, a substrate solution was added to induce an enzymatic color reaction. VEGF content in the samples was estimated by optical density analysis at 450 nm with Synergy H1microplate reader (BioTek, Winooski, VT, USA).

### 2.8. Tissue Histological Analysis

Peritoneal tissue and diaphragm collected from euthanized mice were formalin-fixed, paraffin-embedded and microtome-sectioned (5 μm) for histological analysis using H&E staining to study tumor progression at different timepoints. Pathological analysis was performed on images captured with Leica compound microscope (DM500, Wetzlar, Hesse, Germany) connected with a camera (ICC50 HD, Leica) and analyzed by two independent pathologists.

### 2.9. Immunohistochemistry (IHC) Analysis

Paraffin-embedded tissues of mice euthanized at day 35 were sectioned and subsequently subjected to standard immunohistochemical staining protocol for analysing the effects of angiogenesis and proliferation. All samples were stained with antibodies, anti-CD31 and anti-Ki67. Heat mediated antigen retrieval steps were performed after dewaxing and rehydration steps followed by blocking and washing steps. The samples were then incubated with primary antibody. Super Sensitive™ Polymer HRP IHC Detection System kit (BioGenex, Fremont, CA USA) was used for further processing. Immuno-reactions were visualized with 3,3-diaminobenzidine (DAB) substrate. Microscopic analysis and imaging were done with Leica compound microscope equipped with a camera. A minimum of five random high-power fields of view of each tissue was chosen from all groups and the percentage of diaminobenzidine stained area form each image was analyzed using the NIH Image J software (National Institute of Health, Bethesda, MD, USA).

### 2.10. Preclinical Safety Analysis

Animals were monitored daily for body weight change, food intake, fecal excretion, weakness and inactivity. The animals subjected to surgery were inspected post-mortem for infection at surgery site and incision healing. Peritoneum of animals were closely monitored for tumor nodules, accumulation of blood and ascitic fluid. Blood was collected by post-mortem cardiac puncture and submitted to Idexx Laboratories (North Grafton, MA USA) for whole blood complete blood cell count (CBC) analysis. Hepatotoxicity was studied by measuring serum levels of alanine aminotransferase (ALT) and aspartate aminotransferase (AST) enzymes using ALT and AST reagent kits (Pointe Scientific, Inc. Canton, MI, USA), respectively, following the manufacturer's protocol. Liver and spleen collected from mice were histologically analyzed by H&E staining to study organ toxicity.

### 2.11. Statistical Data Analysis

All data are presented as mean ± standard deviation. Statistical significance was evaluated with the difference in mean values between multiple groups using one-way ANOVA with Tukey post-hoc multiple comparison tests. Statistical significance was set at $p<0.001$ for VEGF analysis and $p < 0.05$ for all other analyses.

## 3. RESULTS

### 3.1. Nanotextile Impant Characterization and *In Vitro* Cytotoxicity of PTX in ID8-VEGF Cells

Scanning electron microscopy images of the nanotextile implants fabricated by adopting the conventional plain weaving technique to weave electrospun yarns of PDS loaded with PTX are shown in Figure 1-A. The effect of PTX on ID8 cells was investigated by an *in vitro* cytotoxicity assay to assess how cell growth is inhibited by PTX in a concentration and time-dependent manner. Figure 1-B shows the effect of cells treated with PTX from both solution and PTX-nanotextile implant groups over 1 to 3 days. Cytotoxicity curves showed that ID8 cells were sensitive to PTX concentrations ranging from 0.5 nM to 2.0 μM. The $IC_{50}$ values for the nanotextile implants and solution were ~45 nM and ~2 nM respectively at 24 h, which decreased with increasing incubation time.

### 3.2. *In Vivo* PTX-release from Nanotextile Implants

Our previous study evaluating tumor progression in ID8-VEGF ovarian tumor model already ascertained the disease state of mice at day 8, owing to the increase in VEGF levels (~20 pg/ml) and Tumor Associated Macrophages (~5%) [34]. Based on this result, PTX-nanotextile was implanted on day 8 and the drug release was quantified by analyzing PTX content in the explanted implant at different timepoints. The *in vivo* PTX-release profile showed a metronomic sustained release and drug availability up to the final euthanasia timepoint of typically one month. While nearly 55 % of the total entrapped PTX was released in a week, ~65 % and 70 % of the drug content was released within 16 and 28 days, respectively (Supplementary Figure 1). These results suggest the ability of the PDS nanotextile implants to release drug for longer durations in the tumor-laden mice peritoneum, which is consistent with our previous findings in healthy animals [30].

### 3.3. *In Vivo* Anti-tumor Efficacy in ID8-VEGF Tumor-Bearing Mice

**3.3.1. Tumor Nodules and Ascitic Fluid Accumulation:** The anti-tumor effects of PTX (20 mg/kg) were evaluated in a time-dependent manner in syngeneic ovarian tumor mice model over 16, 24 and 35 days. IP Injection of ID8-VEGF cells resulted in the formation of multiple tumor nodules in the peritoneum of mice over a span of 35 days. This metastatic tumor progression resulted in peritoneal ascitic fluid accumulation by day 35 in the control groups (untreated and bare nanotextile) [37,38]. Specifically, few tumor nodules and blood traces in peritoneum were observed in the peritoneal tissue and diaphragm of these mice , at day 16 (Supplementary Figure 2 **panel one**). At this timepoint, PTX-solution treated mice showed no tumor nodules, although there were traces of blood in the peritoneal cavity. In contrast, PTX-nanotextile implanted mice peritoneum was totally devoid of tumor

or blood traces. Furthermore, no obvious changes were noticed in the external appearance (especially abdomen) of animals subjected to PTX treatment at day 16.

At day 24, mice in control groups as well as those injected with PTX-solution showed an increase in metastatic lesions in peritoneal tissues and diaphragm, along with presence of blood in the peritoneal cavity (Supplementary Figure 2 **panel two**). In sharp contrast, PTX-nanotextile implanted mice had a clean peritoneum without blood or tumor nodules, presenting a normal external abdominal appearance. By day 35, a subsequent increase in the abdominal circumference was noted for mice of control and PTX-solution groups, with ~3-fold increment in comparison to PTX-nanotextile implanted mice (Figure 2A&B). Extensive tumor metastasis with nodules spread all over the peritoneal cavity, predominantly over the peritoneal tissue and diaphragm, were found for the control groups (Supplementary Figure 3).

Nevertheless, by day 35, a substantial increase in tumor lesions and ascitic fluid accumulation in small volumes was noted for the PTX-solution group albeit its lesser extent relative to control groups. Ascitic fluid volumes of 4.3±1.7 mL, 5.2±1.9 mL, and 1.6±1.2 mL were drained from animals of untreated, bare nanotextile and PTX-solution groups, respectively (Figure 2C). In contrast, PTX-nanotextile implanted mice appeared healthy throughout the treatment period, with no ascitic fluid accumulation in the abdomen (Figure 2A) or tumor nodules in the peritoneum, similar to that of naive mice (Supplementary Figure 3). Additionally, the nanotextile remained intact with no fibrous encapsulation or infection at the sutured site at all timepoints, post-mortem (Supplementary Figure 4). In another experiment wherein the dose of PTX in the nanotextile was increased to 30 mg/kg, significant toxicity was observed and the tumor-bearing animals showed loss of body weight and other consequences of PTX overdose (data not shown).

**3.3.2. VEGF Levels in the Peritoneal Lavage Fluid:** Increased VEGF levels is reported to be a prominent marker for tumor progression in advanced ovarian carcinoma [39,40]. Accordingly, the VEGF levels in peritoneal lavage/ ascitic fluid of mice euthanized at different timepoints were quantified (Figure 2D). Our previous study evaluating tumor progression in ID8-VEGF ovarian cancer mice model had revealed ~36-fold increase in VEGF levels by day 8 (~20 pg/mL), in comparison to that of naive mice without tumor [34]. Herein, the VEGF levels of untreated, tumor-bearing mice (~50 pg/mL) at day 16 displayed a 3-fold and 140-fold increment at days 24 and 35 respectively. The mice implanted with bare nanotextiles also showed a similar trend wherein the VEGF level of ~25 pg/mL at day 16 showed a 4-fold and ~200-fold increment at days 24 and 35 respectively. This clearly illustrates the extent of metastatic tumor progression in the control groups by day 35. In comparison, a relatively higher initial VEGF level in PTX-treated groups (PTX-solution and PTX-nanotextile) was observed at day 16. However, with time, these levels for the PTX-solution group showed a different trend, with a 2-fold decrease on day 24 with respect to day 16, and thereafter a 60-fold enhancement at day 35. On the contrary, PTX-nanotextile implanted mice showed a consistent and gradual decrease in VEGF levels from day 16 to 35, with a 5-fold and 600-fold decrease on days 24 and 35 respectively, relative to control groups (*$p < 0.001$). Importantly, the VEGF level at day 35 for the PTX-nanotextile group

was ~300-fold lower than that of PTX-solution treated mice at the same timepoint and more or less similar to that of naïve mice.

**3.3.3. Metastatic Disease Progression:** The time-dependent metastatic tumor progression in ID8-VEGF mice model as well as the effect of PTX treatment on the same were studied by a detailed histopathological analysis (Figure 3 & Supplementary Table 1). H&E stained images of peritoneal tissue (Figure 3A) and diaphragm (Figure 3B) of naive mice showed intact normal mesothelium, with underlying connective tissues and muscles (Supplementary Figure 5).Untreated, tumor-bearing mice at day 16 showed an irregular mesothelium with malignant cells which progressively thickened by day 24 (Figure 3).

At day 35, the control groups (untreated and bare nanotextile) showed highly irregular mesothelial lining with subsequent multiple layers of pleomorphic malignant cells and underlying fibrosis tissue. Large number of peritoneal tumor deposits with very less normal mesothelium were observed. Specifically, the diaphragm of tumor-bearing mice showed typical histological patterns of serous adenocarcinoma spread, namely micropapillae, nests, glandular and invasive patterns, showing the extent of metastasis (Supplementary Figure 6). PTX-solution injected mice at days 16 and 24 exhibited an onset and spread of tumor, although relatively lesser than control groups. At day 35, a thickened mesothelial lining with intermittent normal mesothelium was observed in this group. Specifically, the diaphragm showed a moderate presence of vacuolated cytoplasm indicating some amount of tumor regression despite the presence of fewer malignant cells. PTX-nanotextile implanted mice at day 16 showed thickened mesothelium with malignant cells, which was considerably reduced by day 24. At day 35, these tissues appeared to be similar to that of naive mice, with its diaphragm revealing the presence of foam cells, which is characteristic of tumor regression [41].

**3.3.4. Expression of Proliferation and Angiogenic Markers:** To further comprehend tumor response to IP PTX treatment, the degree of cell proliferation and angiogenesis were evaluated at day 35 by IHC staining using the proliferation marker Ki-67 and the angiogenic marker CD31 (Figure 4).

Figure 4A clearly reveals an increased immune-expression of Ki-67 as well as CD31 in tumor-bearing control mice in comparison to those treated with PTX. Bare nanotextile implanted mice showed slightly elevated CD31 levels than untreated mice, though statistically these were not significant. The Ki-67 levels were significantly higher for the untreated group (Figure 4B). PTX-solution treatment lowered the Ki-67 immuno-expression in peritoneal tissue and diaphragm of mice by 2.5 and 8-folds, and CD31 levels by 3 and 2-folds, respectively, as compared to untreated animals. A notable difference was observed for the PTX-nanotextileimplanted group wherein a 25-fold and 6-fold reduction in Ki-67 and CD31 levels, respectively, were observed with respect to the control untreated mice (*$p < 0.05$).

## 3.4. Preclinical Safety Assessments

**3.4.1. Hepatotoxicity and CBC Analyses:** To analyze if the PTX treatment induces any acute toxicity effects, serum levels of ALT and AST liver enzymes and CBC at different

timepoints were evaluated. Figure 5 results show that ALT levels in serum for the tumorbearing control mice were slightly elevated in comparison to naive mice, although was not statistically significant. On the contrary, for the PTX-treated groups, the ALT values were minimal and comparable to that of naïve mice (Figure 5A&C). In peritoneal lavage, the higher ALT values for control mice were substantially reduced by ~3 and 5-fold for the PTX-solution and PTX-nanotextile implanted groups, respectively (Figure 5B).

The serum AST values showed a 1.5 and 3-fold reduction for PTX-solution and PTX-nanotextile implanted groups, respectively, in comparison to the untreated controls. Likewise, the lavage AST levels were also reduced by 2-3 and 4-6 folds, respectively (Figure 5D). Whole blood CBC values on day 35 revealed a ~3-fold reduction in RBC and WBC counts for control mice in comparison to naive mice (Figure 5E, F). Specifically, a 6-fold reduction in neutrophils was noted for tumor-bearing mice in comparison to naive mice, while this was not reflected for lymphocyte count (Figure 5G, H). Neutropenia observed for PTX in solution group at day 35, was negated by PTX-nanotextile implanted group, with a ~2.5-fold increment in neutrophil count. Additionally, PTX-nanotextile implanted mice showed RBC and WBC counts comparable to that of naive mice (Figure 5E-H).

**3.4.2. Body Weight Changes:** Mice surgically implanted with the bare and drug-loaded nanotextiles showed minor weight loss immediately following surgery, which was reversed after 5-6 days (Figure 6A). Weight gain, which is indicative of tumor growth, for the untreated control mice was prominent after day 8 of tumor inoculation, while for the bare nanotextile, only after day 17. However, by day 30, a significant weight gain (2-3-fold) was observed in comparison to naïve mice. PTX-solution treated group gained ~1.7-fold weight post-day 11 in comparison to naïve mice, while the PTX-nanotextile treated group did not show any apparent weight gain. By day 35, these animals exhibited ~2-fold weight reduction in comparison to tumor-bearing mice.

**3.4.3. Tissue Histology:** Furthermore, liver and spleen tissues collected upon euthanasia from mice of all groups were analyzed histopathologically for organ toxicity (Figure 6B & Supplementary Table 2). A typical normal morphology of the liver with central veins, sinusoids and radiating hepatocytes were distinctly seen in all groups. However, for animals in the control group (untreated), splenomegaly was noted by day 35 (Supplementary Figure 7). A precise demarcation of red and white pulp was evident in the histological image of naive spleen tissue, while this was not so for the other groups, indicating a possibility of extra-medullary haematopoiesis. Nonetheless, there was a noticeable increase in the red pulp of spleen in PTX-nanotextile implanted mice.

## 4. DISCUSSION

The overarching aim of this study was to establish the *in vivo* efficacy and safety of a combinatorial strategy in advanced OC therapy, wherein, the pharmacokinetic advantages of IP therapy is combined with the anti-tumor effects of low-dose metronomic regimen. To accomplish this, our group developed PTX-loaded woven biodegradable polymeric nanotextile implants from electrospun nanofibrous PDS yarns that could provide sustained and localized IP drug release *in vivo* over a period of >2 months [30]. The electrospun yarns

constituting the implant consisted of several interfaces of high surface area and such a unique nanoarchitecture of this matrix imparted a combinatorial effect of both PTX diffusion and PDS degradation, rendering prolonged drug release. Such a drug eluting depot is advantageous owing to the scalability of the entire fabrication process, amenability to weave textiles of varied sizes, tuneability in drug loading, property of suturability, modulation of drug dosages and release profiles through customization and ease of implantation. This emphasizes the feasibility of nanotextile implants as a clinically translatable option for exploiting the benefits of IP therapy. Also, continuous and sustained drug delivery is proven to enhance the efficacy of chemotherapy by avoiding treatment-free periods, thereby reducing tumor repopulation possibilities [9,23]. Low-dose of chemodrugs administered continuously in a metronomic regimen has reported to impart significant anti-tumor effects by suppressing angiogenesis [24,25].

*In vitro* cytotoxicity studies using PTX-nanotextile and PTX-solution fomulation showed the sensitivity of ID8-VEGF cells to a wide range of PTX concentrations from 0.5 nM to 2.0 μM, which emphasizes the broad therapeutic window of PTX *in vitro* [42,43]. A ~20-fold difference was noted for the $IC_{50}$ values of PTX-nanotextile in comparison to PTX-solution, although both were tested at equivalent concentrations. This could be attributed to the additional toxicity conferred by Cremophor®EL-ethanol, the solvent constituent used in formulating PTX-solution [44].

ID8-VEGF syngeneic orthotopic ovarian tumor model is already established to biologically emulate human epithelial OC progression, with hemorrhagic ascitic fluid accumulation [45]. These serially transformed MOSE cells grow in mice with intact immune system, unlike xenografts, thus mimicking epithelial OC in humans [37,38]. Hence, this model of OC was chosen for the *in vivo* investigation. PTX-nanotextile surgically implanted in the peritoneum of tumor-bearing mice eluted PTX continuously for sustained durations. This metronomic dosing resulted in significant *in vivo* anti-tumor efficacy with less toxicity. Control mice (untreated, bare nanotextile) showed a time-dependent gradual tumor progression in peritoneal cavity, with increase in tumor nodules over the study period of 35 days. The aggressive, metastatic tumor spread at later stages was manifested as abdominal distension due to ascites accumulation in the peritoneum [40]. Post-mortem examination of mice peritoneum at day 16 clearly revealed the anti-tumor effects of PTX from both PTX-solution and PTX-nanotextile groups. However, at day 24, only for mice injected with PTX-solution, prominent tumor nodules and blood traces were found in the peritoneal cavity, implying tumor progression. The short half-life of IP PTX-solution (3 h) which inhibited its retention in the mice peritoneum, might have triggered tumor recurrence at later timepoints, as reported previously [46]. Beyond day 27, ID8 tumor spread was aggressive for control groups with substantial increase in abdominal circumference, correlating with the accumulation of peritoneal ascitic fluid [40]. The disease spread and ascites buildup were also evident for PTX-solution injected mice at later time-points, although the extent of metastasis was lesser than that of PTX-free control groups. On the contrary, a clean peritoneum, devoid of tumor nodules was observed for PTX-nanotextile implanted mice at all timepoints, owing to the continuous elution of PTX from the depot. Animals neither had abdominal distension, nor ascitic fluid formation. Also, the initial burst release of the drug from PTX-nanotextile might have prevented the onset of tumor spread by day 16 through its

cytotoxic activity. Subsequent slow and continuous PTX-release correlating to a metronomic dosing regimen might be responsible for the suppression of tumor progression beyond day 24, owing to the retention of IP PTX-levels for an extended time period in peritoneum [30]. This also underlines the advantages offered by the biphasic drug release profile of PTX-nanotextile wherein the initial burst phase mimics the loading dose currently employed in IP therapy [47,48]. The metronomic phase post burst release aids in maintaining PTX levels at low doses, thereby preventing disease recurrence. This IP pharmacokinetic advantage rendered by PTX-nanotextiles thus conferred superior anti-tumor efficacy over the rapidly clearing IP PTX-solution.

The benefits offered by metronomic dosing are in general attributed to its anti-angiogenic effects, wherein low drug doses damage the tumor endothelial cells [11,32]. VEGF is known to be a major positive regulator for angiogenesis that expands tumor vasculature, and is highly specific for endothelial cells [49], A prominent increase in VEGF levels during OC metastatic progression is known to cause increased vascular permeability of the peritoneal membrane as well as enhanced leakiness of blood vessels in the cavity. Such a scenario is well replicated by ID8-VEGF syngeneic OC model, which is a richly vascularized tumor due to overexpression of the angiogenic factor VEGF [38]. For the control groups, a gradual and substantial increase in VEGF in ascitic fluid was noted over 35 days, indicating the development of an angiogenic vasculature, resulting in the accumulation of malignant ascites [50]. VEGF over-expression in ascitic fluid is therefore a strong predictive marker for poor prognosis and rapid recurrence of late-stage OC [39,51]. For the PTX-treated groups, high VEGF levels at day 16 in contrast to that of control groups, can be attributed to the enhanced VEGF mRNA up-regulation mediated by the bolus dose effect of IP PTX-solution and the initial burst PTX-release from nanotextiles [52,53]. However, the rapid clearance of PTX-solution from peritoneal cavity might have suppressed this high VEGF level by day 24, also indicating tumor regression. Further higher VEGF levels by day 35 for PTX-solution indicate the metastatic progression caused by a possible disease relapse and ascites accumulation. Conversely, PTX-nanotextile group revealed a gradual decline in VEGF after day 16 correlating to its *in vivo* PTX-release profile. The decrease in VEGF levels also imply the suppressive effect of low-dose metronomic PTX released after the burst phase on angiogenesis, ultimately resulting in the complete obliteration of tumor, with no ascites formation [54]. This emphasizes the effectiveness of exposure to low PTX concentrations for a protracted period of time as an anti-angiogenic window for apoptosis induction as well as inhibition of proliferation of vascular endothelial cells [24,55]. Furthermore, the rise in VEGF levels is also directly proportional to increase in tumor cells as ID8-VEGF cells used for tumor inoculation are transfected for overexpressing VEGF. Therefore, the gradual decrease in VEGF levels of PTX-nanotextile group could also be associated with the substantial decrease in tumor.

Pathological observation is the primary reliable determinant used in clinics to evaluate the impact of chemotherapy on tumor growth. Histological analysis of peritoneal tissue and diaphragm of control mice on day 35 revealed proliferated mesothelium with numerous invasive peritoneal implants and highly pleomorphic tumor cells, which is typical of ovarian adenocarcinoma [56,57]. Its invasive nature is pathologically manifested by diverse architectural patterns (micropapillae, irregular glands with round solid nests of cells and

stromal invasion) [58-60], all of which were noticeable in tumor-bearing control mice. Peritoneal tissue of PTX-solution group showed thickened mesothelium with less peritoneal implants, indicating a tumor spread lesser than that of control animals. In contrast, PTX-nanotextile implanted mice showed all cytological features similar to that of naïve mice, emphasizing the complete obliteration of tumor.

Prominent cytologic changes in OC following successful chemotherapy are cytoplasmic alterations like vacuolization and stromal changes with presence of foam cells and foreign body giant cells [41,61,62]. Although the presence of malignant cells in mesothelium indicate tumor spread, cytoplasmic vacuolization noted in certain regions of diaphragm for PTX-solution group at day 35, correlates with the response to PTX-solution therapy. However, for PTX-nanotextile, the appearance of foam cells in the diaphragm indicates a substantial amount of tumor regression [63]. Additionally, these animals exhibited no specific morphological alterations, signifying a very good anti-tumor response to PTX eluted from nanotextile in a slow and sustained manner. Likewise, immunohistochemical evaluation of the cell proliferation marker, Ki-67 and the angiogenic marker CD31 in the tissues of control and treated mice on day 35 reflected the antiproliferative and anti-angiogenic effects of metronomic PTX dosing from nanotextiles, which outweighs the effects of PTX-solution.

From the safety perspective, liver enzyme levels and CBC were used as indicators to evaluate toxicity. ALT and AST levels in serum and lavage of PTX-treated mice did not show any clinical abnormalities [64]. The slightly elevated enzyme levels of PTX-solution injected mice in comparison to PTX-nanotextile group could be attributed to the hematologic toxicity conferred by the PTX bolus dose [65]. CBC results further underlined the non-toxic effect of metronomic dosing from PTX-nanotextile. Leukopenia and neutropenia, the reported dose-dependent hematologic toxicities of the drug as reflected for PTX-solution therapy [66], was completely absent for PTX-nanotextiles, owing to the continuous therapy it offered. Additionally, RBC and WBC levels of PTX-nanotextile implanted mice at day 35 were similar to that of naive mice, ascertaining no toxicity. It can also be inferred that single administration of PTX-solution conferred toxicity issues owing to its bolus dosing as well as the effect of the constituent solvent Cremophor, used for formulating PTX-solution [67,68]. On the contrary, PTX-nanotextile implant woven from yarns of biodegradable and biocompatible PDS is devoid of cremophor and hence does not elicit any toxicity concerns.

Time-dependent weight gain, another acute toxicity indicator, was obvious for the control groups, implying tumor progression with aggressive metastasis and peritoneal ascitic fluid accumulation in the late stages [69]. Control mice thus displayed time-dependent signs of weakness and immobility, with less food intake and abdominal distension. Weight gain of PTX-solution injected animals few days after injection, also correlates to tumor development following its clearance. The relatively stable body weight of mice implanted with PTX-nanotextiles and its similarity to naive mice emphasizes the anti-tumor efficacy offered by such depots which continuously elute the drug, with no toxic effects. Additionally, no histological signs of toxicity were observed in the liver and spleen of mice from all groups. Extra-medullary haematopoiesis observed in the spleen of mice can be correlated to the

presence of tumor in control groups and the impact of chemotherapy in PTX-treated mice [70,71]. Furthermore, animals implanted with PTX-nanotextiles were healthy throughout the treatment period and did not show any signs of weakness or physical wasting and abdominal distension. The same amount of drug contained in a single dose of PTX-solution upon continuous administration as metronomic low-doses through an implant, mitigates all toxicity issues. It therefore represents a safer alternative to the conventional IP bolus dosing for implementing intraperitoneal therapy. Overall, our results confirm that low-dose metronomic release for a sustained period provided by PTX-nanotextiles yield superior anti-tumor efficacy without any toxic side effects.

## 5. CONCLUSIONS

In this study, we thus demonstrate that sustained metronomic dosing of PTX from woven nanotextile PDS implants could confer enhanced anti-tumor therapeutic benefits in syngeneic OC model via suppression of VEGF-mediated angiogenesis and metastatic progression. Moreover, toxic effects otherwise imparted by systemic PTX-therapy could be mitigated by this low-dose IP therapy approach. Our preclinical results thus establish the effectiveness of combining metronomic PTX dosing with the capability of woven PDS nanotextiles to provide sustained intraperitoneal drug delivery, for addressing late-stage metastasis and recurrence of peritoneal malignancies. This concept can very well be extended to a wide range of polymers and chemotherapeutic drugs that would ultimately enhance the pharmacokinetic benefits of intraperitoneal therapy, especially in advanced and refractory OC patients. Therefore, nanotextile depots hold immense potential to improve the long-term clinical outcome of OC therapy.

## Supplementary Material

Refer to Web version on PubMed Central for supplementary material.

## ACKNOWLEDGEMENTS

The authors also acknowledge the assistance provided by Dr. Raghunath Narayanan and Dr. Rohit (Consultant Pathologists, Med-Helix Diagnostics, Pvt Ltd., Kochi, India) for tissue histological analysis.

FUNDING

Financial support for this work was provided by the United States National Cancer Institute of the National Institute of Health through grants R21-CA179652 and R56-CA198492, and the Northeastern University-Dana Farber Cancer Center Joint Program on Cancer Drug Development. Additional funding was obtained from the Pilot Project Grants, Program for Young Investigators in Cancer Biology of the Department of Biotechnology, Government of India. SP acknowledges DST-INSPIRE, Government of India for her SRF Fellowship and Amrita Vishwa Vidyapeetham for PhD Scholar's Fellowship (2017).

## REFERENCES

[1]. Ahmed N, Abubaker K, Findlay JK, Ovarian cancer stem cells: Molecular concepts and relevance as therapeutic targets, Mol. Aspects Med.39 (2014)110–125. doi:10.1016/j.mam.2013.06.002. [PubMed: 23811037]

[2]. American Cancer Society, What are the key statistics about ovarian cancer?, Https://Www.Cancer.Org/Cancer/Ovarian-Cancer/about/Key-Statistics.Html. (2018). https://

www.cancer.org/cancer/ovarian-cancer/about/key-statistics.html%5Cnhttp://www.cancer.org/cancer/ovariancancer/detailedguide/ovarian-cancer-key-statistics.

[3]. de A. Chuffa LG, Reiter RJ, Lupi LA, Melatonin as a promising agent to treat ovarian cancer: Molecular mechanisms, Carcinogenesis. 38 (2017) 945–952. doi:10.1093/carcin/bgx054. [PubMed: 28575150]

[4]. Cannistra SA, Cancer of the Ovary, N. Engl. J. Med. 351 (2004) 2519–2529. doi: 10.1056/NEJMra041842. [PubMed: 15590954]

[5]. Armstrong DK, Bundy B, Winzel L, Huang HQ Baergen R, Lele S, Copeland LJ, Walker JL, Burger RA, Intraperitoneal Cisplatin and Paclitaxel in Ovarian Cancer, Obstet. Gynecol. Surv. 61 (2006) 240–242. doi:10.1097/01.ogx.0000206353.22975.c5.

[6]. Narod S, Can advanced-stage ovarian cancer be cured?, Nat. Rev. Clin. Oncol. 13 (2016) 255. [PubMed: 26787282]

[7]. Huang Z, Yan H, Chavan D, Yuan Z, Yang X Zhang Y Song K, Kong B Effective treatment of a patient with stage IV ovarian cancer: A case report, Oncol. Lett. 15 (2018) 588–591. doi: 10.3892/ol.2017.7285. [PubMed: 29285202]

[8]. Zhidkov N, Intraperitoneal , Continuous Carboplatin Delivery for the Treatment of Ovarian Cancer, Mol. Pharm. 10 (2013) 3315–3322. [PubMed: 23924289]

[9]. Vassileva V, Allen CJ, Piquette-Miller M, Effects of sustained and intermittent paclitaxel therapy on tumor repopulation in ovarian cancer., Mol. Cancer Ther. 7 (2008) 630–637. doi: 10.1158/1535-7163.MCT-07-2117. [PubMed: 18347149]

[10]. Iyer AK, Singh A, Ganta S, Amiji MM, Role of integrated cancer nanomedicine in overcoming drug resistance, Elsevier B.V., 2013. doi:10.1016/j.addr.2013.07.012.

[11]. Saad M, Minko T, Co-delivery of siRNA and an anticancer drug for treatment of multidrug-resistant cancer, Nanomedicine (Lond). 3 (2008) 761–776. [PubMed: 19025451]

[12]. Milane L, Ganesh S, Shah S, Duan Z, Amiji M, Multi-Modal Strategies for Overcoming Tumor Drug Resistance: Hypoxia, Warburg's Effect, Stem Cells, and Multifunctional Nanotechnology, J. Control. Release. 155 (2011) 237–247. doi:10.1016/j.immuni.2010.12.017.Two-stage. [PubMed: 21497176]

[13]. Cojoc M, Mäbert K, Muders MH, Dubrovska A, A role for cancer stem cells in therapy resistance: Cellular and molecular mechanisms, Semin. Cancer Biol. 31 (2015) 16–27. doi: 10.1016/j.semcancer.2014.06.004. [PubMed: 24956577]

[14]. Williamson SK, Johnson GA, Maulhardt HA, Moore KM, McMeekin DS, Schulz T, Reed GA, Roby KF, Mackay CB, Smith HJ, Weir SJ, Wick JA, Markman M, diZerega GS, Baltezor MJ, Deceduell JECJ, A phase I study of intraperitoneal nanoparticulate paclitaxel (Nanotax® ) in patients with peritoneal malignancies, Cancer Chemother. Pharmacol. 75 (2015) 1075–1087.doi: 10.1038/leu.2015.334.FOXM1. [PubMed: 25898813]

[15]. Padmakumar S, Parayath N, Leslie F, Nair SV, Menon D, Amiji MM, Intraperitoneal chemotherapy for ovarian cancer using sustained-release implantable devices, Expert Opin. Drug Deliv. 15 (2018) 481–94. doi:10.1080/17425247.2018.1446938. [PubMed: 29488406]

[16]. Helm CW, Ports and complications for intraperitoneal chemotherapy delivery, BJOG An Int. J. Obstet. Gynaecol. 119 (2011) 150–159. doi:10.1111/j.1471-0528.2011.03179.x.

[17]. Davis AJ, Tannock IF, Repopulation of tumour cells between cycles of chemotherapy: A neglected factor, Lancet Oncol. 1 (2000) 86–93. doi:10.1016/S1470-2045(00)00019-X. [PubMed: 11905673]

[18]. Vassileva V, Moriyarna EH, De Souza R, Grant J, Allen CJ, Wilson BC, Piquette-Miller M, Efficacy assessment of sustained intraperitoneal paclitaxel therapy in a murine model of ovarian cancer using bioluminescent imaging., Br. J. Cancer. 99 (2008) 2037–2043. doi:10.1038/sj.bjc.6604803. [PubMed: 19034272]

[19]. Colby AH, Oberlies NH, Pearce CJ, Herrera VLM, Colson YL, Grinstafi MW; Nanoparticle Drug Delivery Systems for Peritoneal Cancers: A Case Study of the Design, Characterization, and Development of the Expansile Nanoparticle, Wiley Interdiscip Rev Nanomed Nanobiotechnol. 9 (2017) 1–32. doi:10.1002/wnan.1451.Nanoparticle.

[20]. Yang M, Yu T, Wood J, Wang YY, Tang BC, Zeng Q, Simons BW, Fu J, Chuang CM, Lai SK, Wu TC, Hung CF, Hanes J, Intraperitoneal delivery of paclitaxel by poly(ether-anhydride)

microspheres effectively suppresses tumor growth in a murine metastatic ovarian cancer model, Drug Deliv. Transl. Res. 4 (2014) 203–209. doi:10.1007/s13346-013-0190-7. [PubMed: 24816829]

[21]. Sun B, Taha MS, Ramsey B, Torregrosa-Allen S, Elzey BD, Yeo Y, Intraperitoneal chemotherapy of ovarian cancer by hydrogel depot of paclitaxel nanocrystals, J. Control. Release. 235 (2016)91–98. doi:10.1016/j.jconrel.2016.05.056. [PubMed: 27238443]

[22]. Bajaj G, Kim MR, Mohammed SI, Yeo Y, Hyaluronic acid-based hydrogel for regional delivery of paclitaxel to intraperitoneal tumors, J. Control. Release. 158 (2012) 386–392. doi:10.1016/j.jconrel.2011.12.001. [PubMed: 22178261]

[23]. Ye H, Tanenbaum LM, Na YJ, Mantzavinou A, Fulci G, Del Carmen MG, Birrer MJ, Cima MJ, Sustained, low-dose intraperitoneal cisplatin improves treatment outcome in ovarian cancer mouse models, J. Control. Release. 220 (2015) 358–367. doi:10.1016/j.jconrel.2015.11.001. [PubMed: 26548976]

[24]. Kerbel RS, Kamen BA, The anti-angiogenic basis of metronomic chemotherapy, Nat. Rev. Cancer. 4 (2004) 423–436. doi:10.1038/nrc1369. [PubMed: 15170445]

[25]. Biziota E, Mavroeidis L, Hatzimichael E, Pappas P, Metronomic chemotherapy: A potent macerator of cancer by inducing angiogenesis suppression and antitumor immune activation, Cancer Lett. 400(2017). doi:10.1016/j.canlet.2016.12.018.

[26]. Hashimoto K, Man S, Xu P, Cruz-Munoz W, Tang T, Kumar R, Kerbel RS, Potent Preclinical Impact of Metronomic Low-Dose Oral Topotecan Combined with the Antiangiogenic Drug Pazopanib for the Treatment of Ovarian Cancer, Mol. Cancer Ther. 9 (2010) 996–1006. doi:10.1158/1535-7163.MCT-09-0960. [PubMed: 20371722]

[27]. Merritt WM, Danes CG, Shahzad MMK, Lin YG, Kamat AA, Han LY, Spannuth WA, Nick AM, Mangala LS, Stone RL, Hye SK, Gershenson DM, Jaffe RB, Coleman RL, Chandra J, Sood AK, Anti-angiogenic properties of metronomic topotecan in ovarian carcinoma, Cancer Biol. Ther. 8 (2009) 1596–1603. doi:10.4161/cbt.8.16.9004. [PubMed: 19738426]

[28]. Samaritani R, Corrado G, Vizza E, Sbiroli C, Cyclophosphamide “metronomic” chemotherapy for palliative treatment of a young patient with advanced epithelial ovarian cancer, BMC Cancer. 7 (2007)3–8. doi:10.1186/1471-2407-7-65. [PubMed: 17201909]

[29]. Amoozgar Z, Wang L, Brandstoetter T, Wallis SS, Wilson EM, Goldberg MS, Dual-layer surface coating of PLGA-based nanoparticles provides slow-release drug delivery to achieve metronomic therapy in a paclitaxel-resistant murine ovarian cancer model, Biomacromolecules. 15 (2014) 4187–4194. doi:10.1021/bm5011933. [PubMed: 25251833]

[30]. Padmakumar S, Paul-Prasanth B, Pavithran K, Vijaykumar D, Rajanbabu A, Sivanarayanan T, Kadakia E, Amiji MM, Nair SV, Menon D, Long-term drug delivery using implantable electrospun woven polymeric Nanotextiles, Nanomedicine Nanotechnology, Biol. Med. 15 (2019) 274–284. doi:10.1016/J.NANO.2018.10.002.

[31]. Joseph J, Nair SV, Menon D, Integrating Substrateless Electrospinning with Textile Technology for Creating Biodegradable Three-Dimensional Structures, Nano Lett. 15 (2015) 5420–5426. doi:10.1021/acs.nanolett.5b01815. [PubMed: 26214718]

[32]. Padmakumar S, Joseph J, Neppalli MH, Mathew SE, V Nair S, Shankarappa SA, Menon D, Electrospun Polymeric Core-sheath Yams as Drug Eluting Surgical Sutures, ACS Appl. Mater. Interfaces. 8 (2016) 6925–6934. doi:10.1021/acsami.6b00874. [PubMed: 26936629]

[33]. ISO 10993- 5, Biological evaluation of medical devices — Part 5: Tests for in vitro cytotoxicity, ISO (the Int. Organ. Stand (2009).

[34]. Parayath NN, Gandham SK, Leslie F, Amiji MM, Enhancement of Therapeutic Efficacy in Epithelial Ovarian Cancer with Combination microRNA 125b-Based Tumor-Associated Macrophage Repolarization and Cytotoxic Chemotherapy., Cancer Lett, (under Rev. (2019).

[35]. Bruixola G, Domingo S, Di h.R, Caballero J, Feasibility and Safety of a Modified Outpatient Regimen With Intravenous / Intraperitoneal Chemotherapy for Optimally Debulked Stage III Ovarian Cancer, 25(2015) 214–221. doi:10.1097/IGC.0000000000000330.

[36]. Markman M, Walker JL, Intraperitoneal chemotherapy of ovarian cancer: A review, with a focus on practical aspects of treatment, J. Clin. Oncol. 24 (2006) 988–994. doi:10.1200/JCO.2005.05.2456. [PubMed: 16461779]

[37]. Roby KF, Taylor CC, Sweetwood JP, Cheng Y, Pace JL, Tawfik O, Persons DL, Smith PG, Terranova PF, Development of a syngeneic mouse model for events related to ovarian cancer, Carcinogenesis. 21 (2000) 585–591. doi:10.1093/carcin/21.4.585. [PubMed: 10753190]

[38]. Cho S, Sun Y, Soisson AP, Dodson MK, Peterson CM, Jarboe EA, Kennedy AM, Janat-amsbury MM, Characterization and Evaluation of Pre-clinical Suitability of a Syngeneic Orthotopic Mouse Ovarian Cancer Model, Anticancer Res. 33 (2013) 1317–1324. [PubMed: 23564768]

[39]. Ogawa S, Kaku T, Kobayashi H, Hirakawa T, Ohishi Y, Kinukawa N, Nakano H, Prognostic significance of microvessel density, vascular cuffing and vascular endothelial growth factor expression in ovarian carcinoma: A special review for clear cell adenocarcinoma, Cancer Lett. 176(2002) 111–118. doi:10.1016/S0304-3835(01)00754-6. [PubMed: 11790460]

[40]. Janát-Amsbury MM, Yockman JW, Anderson ML, Kieback DG, Kim SW, Comparison of ID8 MOSE and VEGF-modified ID8 cell lines in an immunocompetent animal model for human ovarian cancer, Anticancer Res. 26 (2006) 2785–2789. [PubMed: 16886597]

[41]. McCluggage WG, Lyness RW, Atkinson RJ, Dobbs SP, Harley I, McClelland HR, Price JH, Morphological effects of chemotherapy on ovarian carcinoma, J. Clin. Pathol. 55 (2002) 27–31. doi:10.1136/jcp.55.1.27. [PubMed: 11825920]

[42]. Wang J, Lou P, Lesniewski R, Henkin J, Paclitaxel at ultra low concentrations inhibits angiogenesis without affecting cellular microtubule assembly, Anticancer. Drugs. 14 (2003) 13–19. doi:10.1097/00001813-200301000-00003. [PubMed: 12544254]

[43]. Dong X, Mattingly CA, Tseng MT, Cho MJ, Liu Y, Adams VR, Mumper RJ, Doxorubicin and paclitaxel-loaded lipid-based nanoparticles overcome multidrug resistance by inhibiting P-glycoprotein and depleting ATP, Cancer Res. 69 (2009) 3918–3926. doi: 10.1158/0008-5472.CAN-08-2747. [PubMed: 19383919]

[44]. Csóka K, Dhar S, Fridborg H Larsson R, Nygren P, Differential activity of Cremophor EL and paclitaxel in patients' tumor cells and human carcinoma cell lines in vitro., Cancer. 79 (1997) 1225–1233. doi:10.1002/(SICI)1097-0142(19970315)79:6<1225::AID-CNCR23>3.0.CO;2-0. [PubMed: 9070502]

[45]. Fong MY Kakar SS, Ovarian cancer mouse models: A summary of current models and their limitations, J. Ovarian Res. 2 (2009) 1–8. doi: 10.1186/1757-2215-2-12. [PubMed: 19144154]

[46]. Innocenti F, Danesi R, Di Paolo A, Agen C, Nardird D, Bocd G, Del Tacca M, Plasma and tissue disposition of paclitaxel (taxol) after intraperitoneal administration in mice., Drug Metab. Dispos. 23 (1995) 713–717. [PubMed: 7587959]

[47]. Gilmore D, Schulz M, Liu R, Zubris KAV, Padera RF, Catalano PJ, Grinstafi MW; Colson YL, Cytoreductive Surgery and Intraoperative Administration of Paclitaxel-loaded Expansile Nanoparticles Delay Tumor Recurrence in Ovarian Carcinoma, Ann. Surg. Oncol. 20 (2013) 1684–1693. doi:10.1245/s10434-012-2696-5. [PubMed: 23128939]

[48]. Armstrong DK, Administration Guidelines for Intraperitoneal Chemotherapy for Ovarian Cancer, in: Intraperitoneal Ther. Ovarian Cancer, 2010: pp. 89–94. doi:10.1007/978-3-642-12130-2_8.

[49]. Ferrara N, Vascular endothelial growth factor as a target for anticancer therapy., Oncologist. 9 Suppl 1 (2004)2–10. doi:10.1634/THEONCOLOGIST.9-SUPPL_1-2. [PubMed: 15178810]

[50]. Masoumi Moghaddam S, Amini A, Morris DL, Pourgholami MH, Significance of vascular endothelial growth factor in growth and peritoneal dissemination of ovarian cancer, Cancer Metastasis Rev. 31 (2012) 143–162. doi:10.1007/s10555-011-9337-5. [PubMed: 22101807]

[51]. Kipps E, Tan DSP, Kaye SB, Meeting the challenge of ascites in ovarian cancer: new avenues for therapy and research, Nat. Rev. Cancer. 13 (2013) 273–282. doi:10.1038/nrc3432. [PubMed: 23426401]

[52]. Choi EK, Kim SW, Nam EJ, Paek J, Yim GW, Kang MH, Kim YT, Differential effect of intraperitoneal albendazole and paclitaxel on ascites formation and expression of vascular endothelial growth factor in ovarian cancer cell-bearing athymic nude mice, Reprod. Sci. 18 (2011) 763–771. doi:10.1177/1933719111398142. [PubMed: 21421899]

[53]. Kim HS, Oh JM, Jin DH, Yang K-H, Moon E-Y, Paclitaxel induces vascular endothelial growth factor expression through reactive oxygen species production., Pharmacology. 81 (2008) 317–24. doi:10.1159/000119756. [PubMed: 18322419]

[54]. Browder T, Butterfield CE, Kräling BM Shi B, Marshall B, O'Reilly MS, Folkman J, Antiangiogenic scheduling of chemotherapy improves efficacy against experimental drug-resistant cancer, Cancer Res. 60 (2000) 1878–1886. [PubMed: 10766175]

[55]. Bocci G, Nicolaou KC, Kerbel RS, Protracted Low-Dose Effects on Human Endothelial Cell Proliferation and Survival in Vitro Reveal a Selective Antiangiogenic Window for Various Chemotherapeutic Drugs 1, Cancer Res. 62 (2002) 6938–6943. [PubMed: 12460910]

[56]. Zeren EH, Demirag F Benign and malignant mesothelial proliferation, Surg. Pathol. Clin. 3 (2010) 83–107. doi:10.1016/j.path.2010.03.010. [PubMed: 26839028]

[57]. Gershenson DM, Silva EG, Serous ovarian tumors of low malignant potential with peritoneal implants, Cancer. 65 (1990). doi:10.1002/1097-0142(19900201)65:3<578::AID-CNCR2820650332>3.0.CO;2-N.

[58]. Vang R Shih le-M., Kurman RJ, Ovarian low-grade and high-grade serous carcinoma: pathogenesis, clinicopathologic and molecular biologic features, and diagnostic problems, Adv. Anat. Pathol. 16 (2009) 267–282. doi:10.1097/PAP.0b013e3181b4fffa.OVARIAN. [PubMed: 19700937]

[59]. Estrella JS, Woli JK; Deavers MT, Ovarian Serous Carcinoma Associated With a Distinct "Corded and Hyalinized" Pattern, Arch. Pathol. Lab. Med. 137 (2013) 275–279. doi:10.5858/arpa.2011-0200-CR. [PubMed: 23368871]

[60]. Greenaway J, Moorehead R, Shaw P, Petrik J, Epithelial-stromal interaction increases cell proliferation, survival and tumorigenicity in a mouse model of human epithelial ovarian cancer, Gynecol. Oncol. 108 (2008) 385–394. doi:10.1016/j.ygyno.2007.10.035. [PubMed: 18036641]

[61]. Tiwana KK, Nibhoria S, Kaur M, Monga T, Gupta R, Postchemotherapy Histopathological Evaluation of Ovarian Carcinoma: A 40-Case Study, Chemother. Res. Pract. 2015 (2015) 1–4. doi: 10.1155/2015/197871.

[62]. Sethi D, Sen R, Parshad S, Khetarpal S, Garg M Sen J, Histopathologic changes following neoadjuvant chemotherapy in various malignancies, Int. J. Appl. Basic Med. Res. (2012) 111–6. doi:10.4103/0019-509X.112301. [PubMed: 23776823]

[63]. Sassen S, Schmalfeldt B, Avril N, Kuhn W, Busch R, Holler H, Fend F, Nahrig J, Histopathologic assessment of tumor regression after neoadjuvant chemotherapy in advanced-stage ovarian cancer, Hum. Pathol. 38 (2007) 926–934. doi:10.1016/j.humpath.2006.12.008. [PubMed: 17397905]

[64]. Fernández I, Peña A, Del Teso N, Pérez V, Rodríguez-Cuesta J, Clinical biochemistry parameters in C57BL/6J mice after blood collection from the submandibular vein and retroorbital plexus., J. Am. Assoc. Lab. Anim. Sci. 49 (2010) 202–6. doi:10.3928/02793695-20100202-06. [PubMed: 20353696]

[65]. LiverTox - Clinical and Research Information on Drug-Induced Liver Injury https://livertox.nih.gov/Paclitaxel.htm, Natl. Inst. Heal. U.S. Dep. Heal. Hum. Serv. (2018).

[66]. Marupudi NI, Han JE, Li KW, Renard VM, Tyler BM, Brem H, Paclitaxel: a review of adverse toxicities and novel delivery strategies, Expert Opin. Drug Safety, 6(5), 609–621. 6(2007) 609–621.

[67]. Xu S, Fan H, Yin L, Zhang J Dong A Deng L Tang H Thermosensitive hydrogel system assembled by PTX-loaded copolymer nanoparticles for sustained intraperitoneal chemotherapy of peritoneal carcinomatosis, Eur. J. Pharm. Biopharm. 104 (2016) 251–259. doi:10.1016/j.ejpb.2016.05.010. [PubMed: 27185379]

[68]. Gelderblom H, Verweij J, Nooter K, Sparreboom A, Cremophor EL: the drawbacks and advantages of vehicle selection for drug formulation, Eur. J. Cancer. 37 (2001) 1590–1598. [PubMed: 11527683]

[69]. Arauchi A, Yang C-H Cho S, Jarboe EA, Peterson CM, Bae YH, Okano T, Janat-Amsbury MM, An Immunocompetent, Orthotopic Mouse Model of Epithelial Ovarian Cancer Utilizing Tissue Engineered Tumor Cell Sheets, Tissue Eng. Part C Methods. 21 (2015) 23–34. doi:10.1089/ten.tec.2014.0040. [PubMed: 24745555]

[70]. Suttie AW, Histopathology of the Spleen, Toxicol. Pathol. 34 (2006) 466–503. doi: 10.1080/01926230600867750. [PubMed: 17067940]

[71]. Wang J Darvishian F, Extramedullary hematopoiesis in breast after neoadjuvant chemotherapy for breast carcinoma, Ann. Clin. Lab. Sci. 36 (2006) 475–478. [PubMed: 17127738]

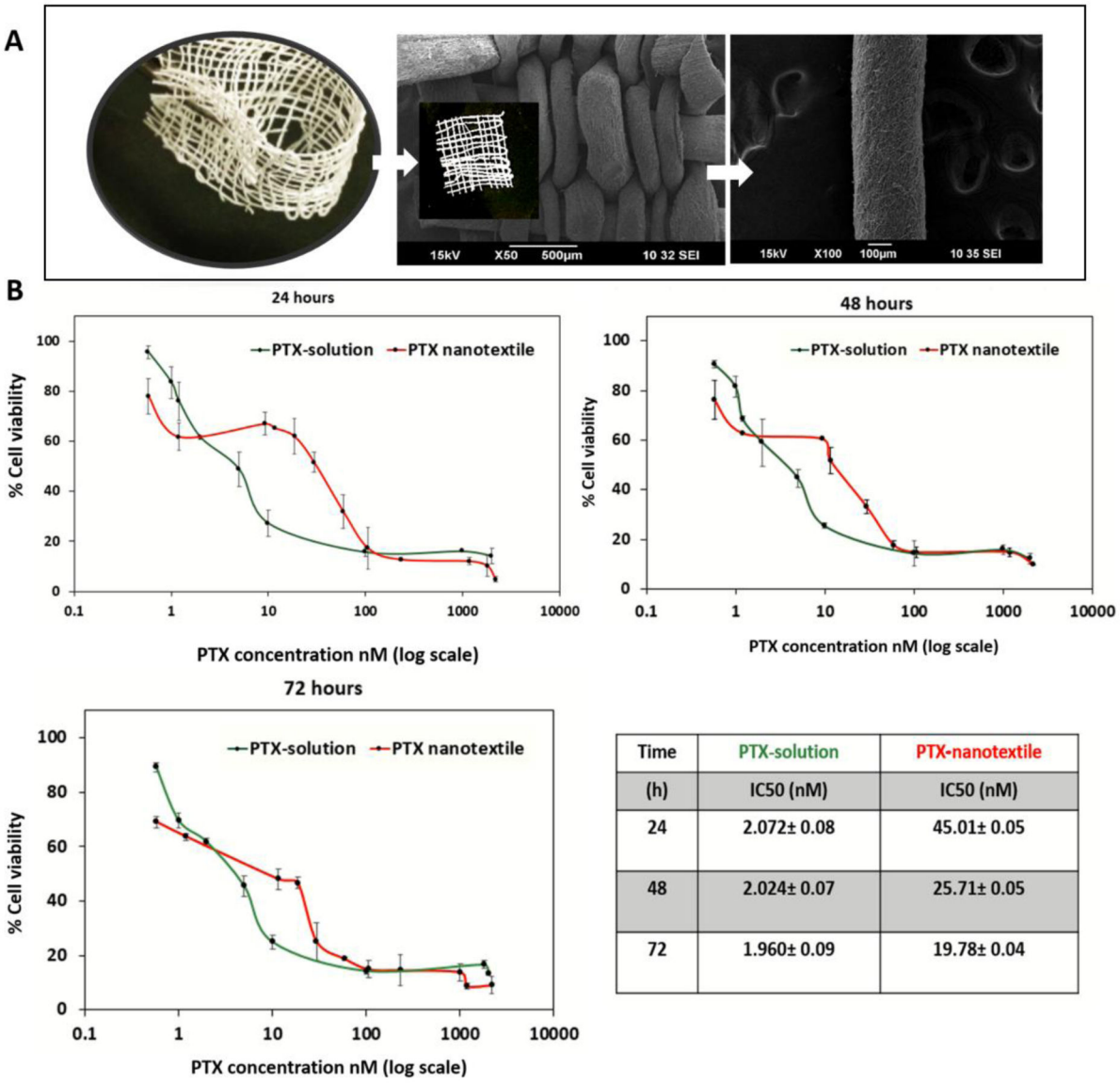


| Time | PTX-solution | PTX-nanotextile |
|---|---|---|
| (h) | IC50 (nM) | IC50 (nM) |
| 24 | 2.072± 0.08 | 45.01± 0.05 |
| 48 | 2.024± 0.07 | 25.71± 0.05 |
| 72 | 1.960± 0.09 | 19.78± 0.04 |

**Figure 1. Nanotextile implant and *in vitro* cytotoxicity of PTX in ID8-VEGF cells.**

**(A)** Optical and scanning electron microscopy images of paclitaxel (PTX)-loaded polydioxanone (PDS) yarn and woven nanotextile implant (inset image) **(B)** The plots of ID8-VEGF cell viability versus PTX concentration administered in solution and from nanotextiles incubated for 24, 48 and72 h. The PTX $IC_{50}$ values were calculated and shown in the table.

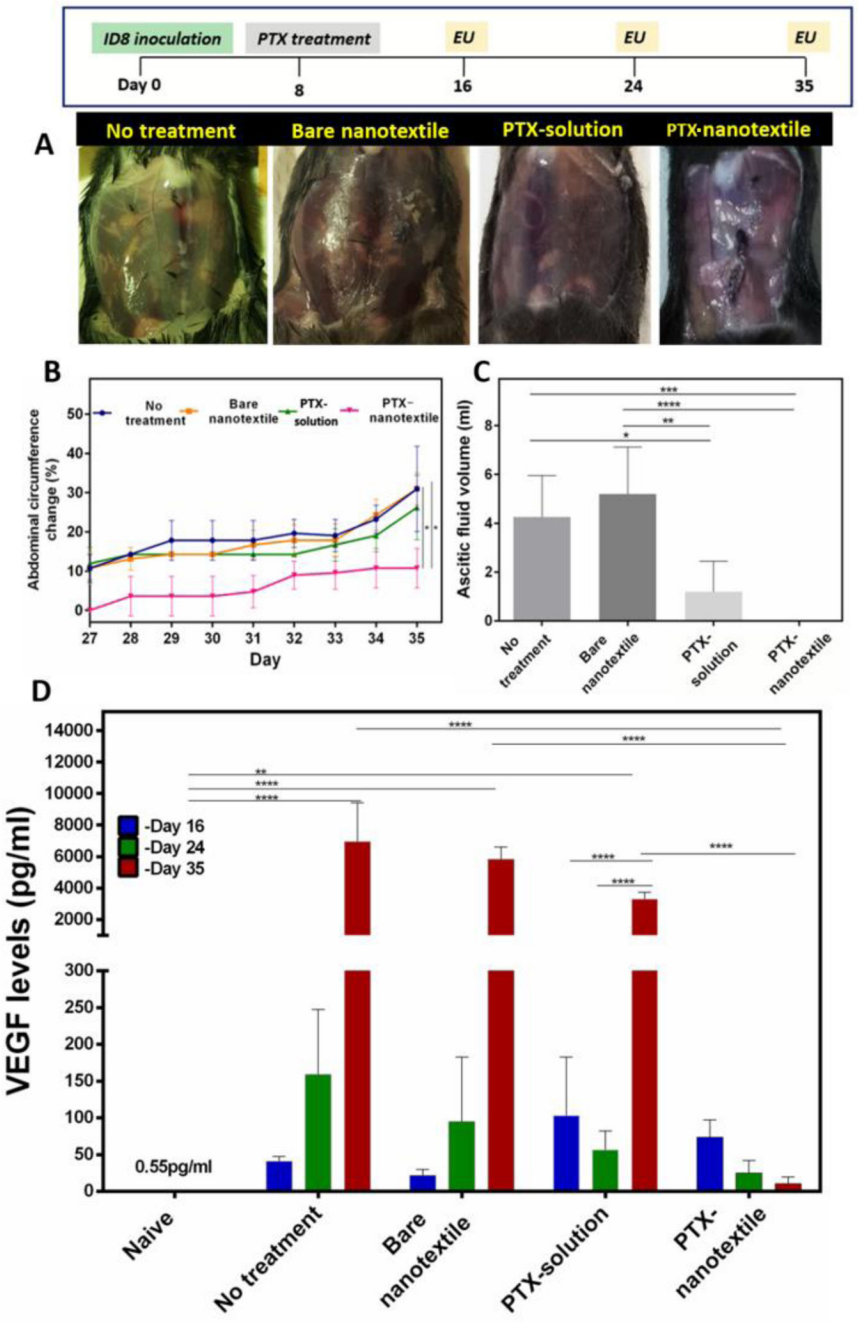


**Figure 2.** ***In vivo*** **anti-tumor efficacy in ID8-VEGF tumor-bearing mice.**

**(A)** Abdominal images of mice upon euthanasia (EU) at day 35 **(B)** Abdominal circumference plotted as a function of time. **(C)** Ascitic fluid collected from mice at day 35 and **(D)** VEGF levels in peritoneal lavage/ fluid of mice at different timepoints. Data shown are mean±S.D., n = 5 per group per time-point (*p <0.05 for ascites volume, *p <0.001 for VEGF analysis).

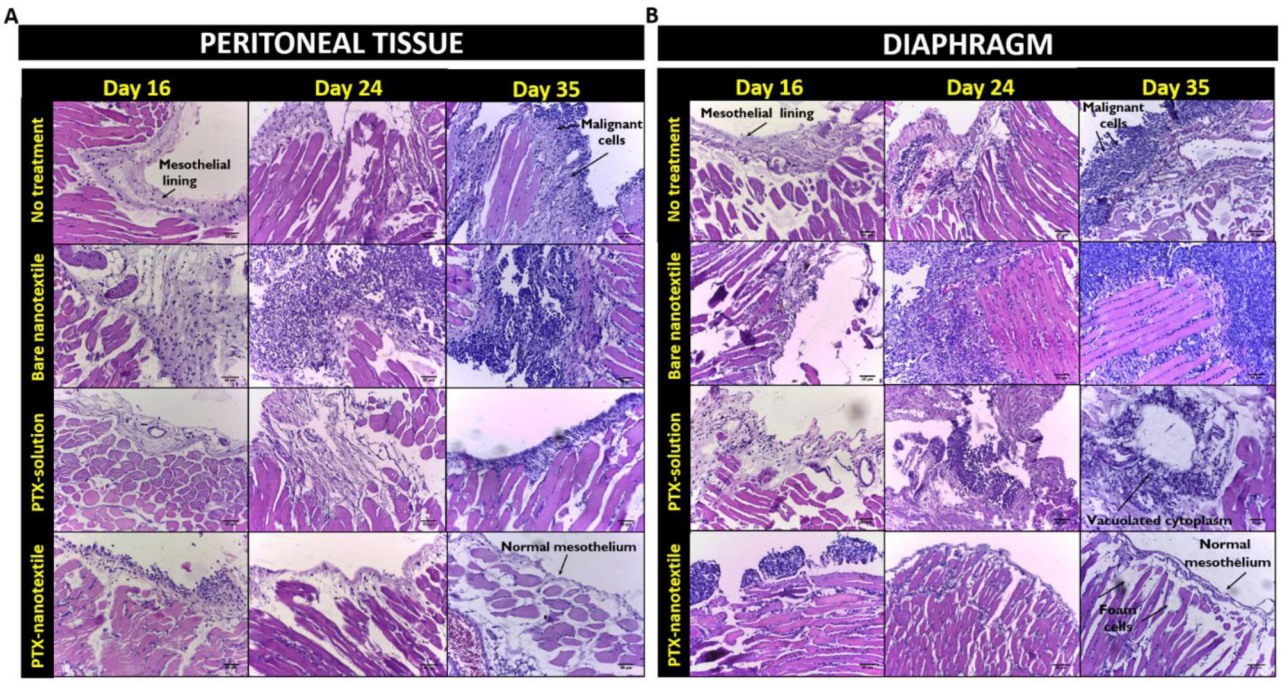


**Figure 3. Metastatic disease progression.**

Hematoxylin and eosin (H&E) histological assessment of **(A)** peritoneal tissue and **(B)** diaphragm of mice from control and treatment groups at days 16, 24 and 35. Scale bar : 50 μm.

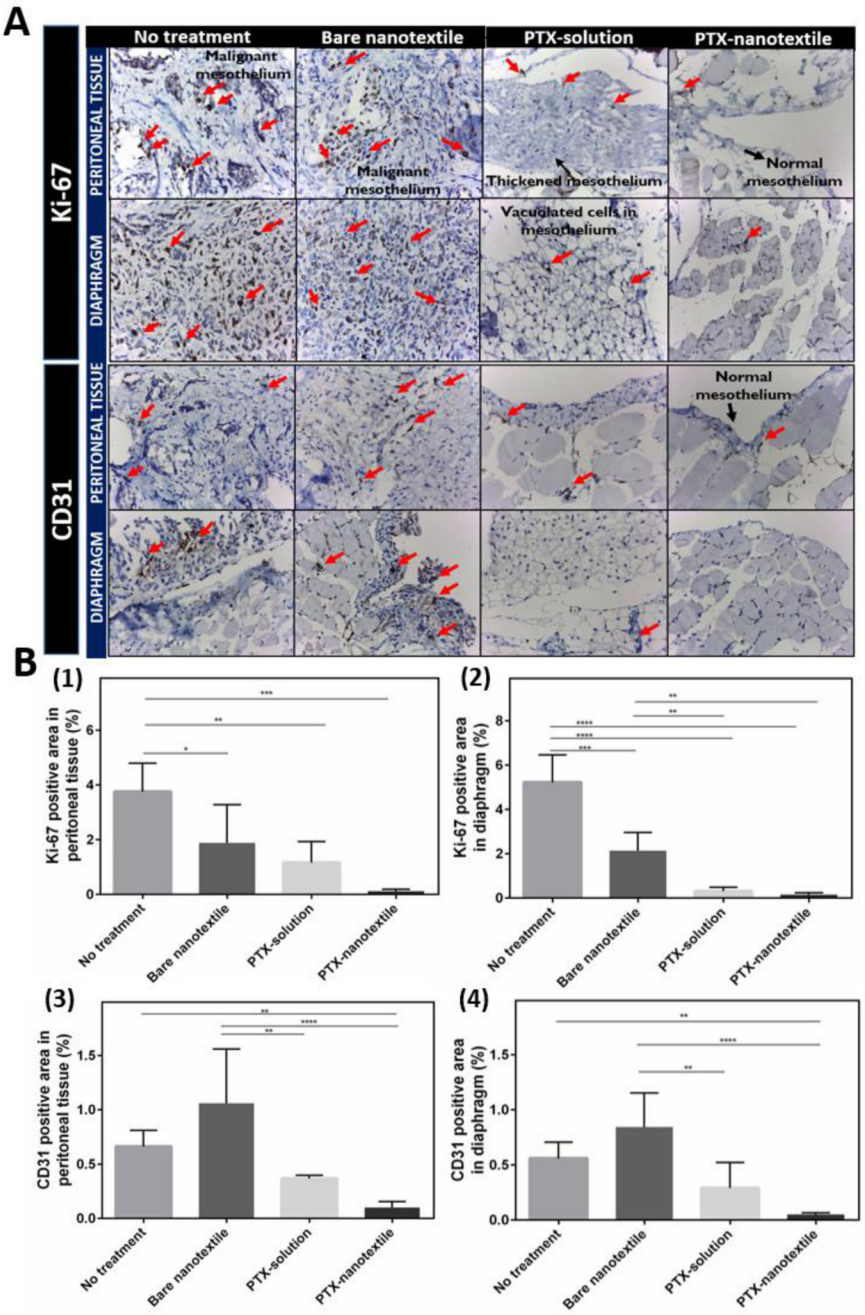


**Figure 4. Expression of proliferation and angiogenic markers.**

**(A)** Immunohistochemistry (IHC) microscopic analysis at 40X magnification showing the expression of proliferation (Ki-67) and angiogenic (CD31) markers in formalin- fixed, paraffin-embedded peritoneal tissue and diaphragm of mice from control and treatment groups euthanized on day 35. **(B)** Semiquantitative analysis of diaminobenzidine stained positive area from the IHC images for Ki-67 and CD31 expression using NIH Image J software.

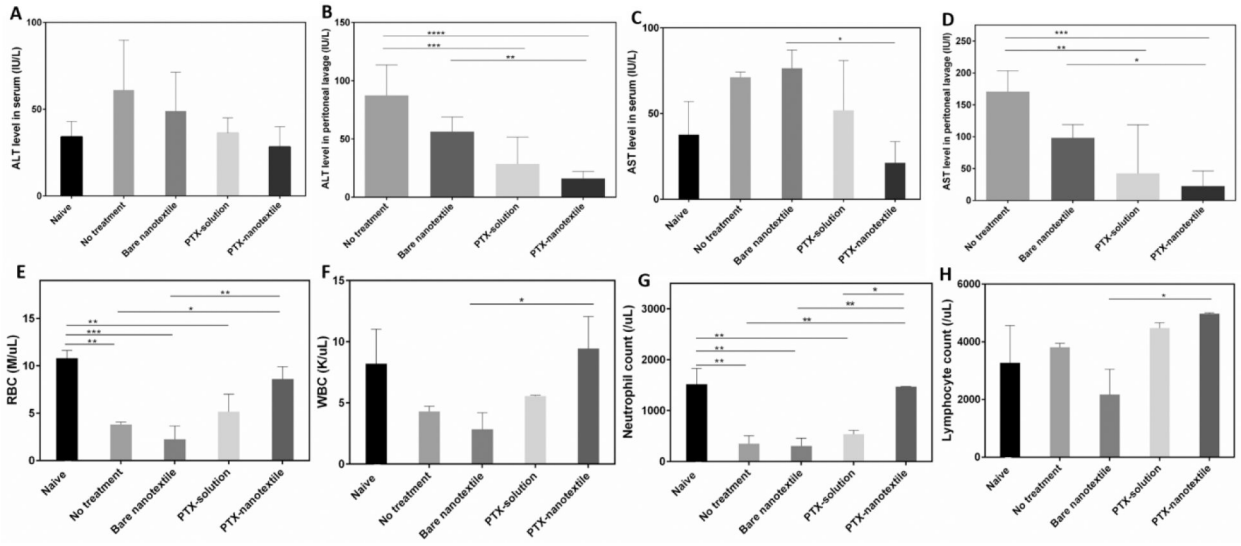


**Figure 5. Liver enzyme levels and complete blood cell countanalyses.**

Alanine aminotransferase (ALT) levels in the **(A)** serum and **(B)** perineal lavage as well as aspartate aminotransferase (AST) levels in the **(C)** serum and **(D)** peritnoneallavage.Complete blood cell count (CBC) analysis showing counts of **(A)** red blood cells (RBC) **(B)** white blood cells (WBC), **(C)** neutrophils, and **(D)** lymphocytes. Data shown are mean ± SD (n =3 per group) (*$p < 0.05$).

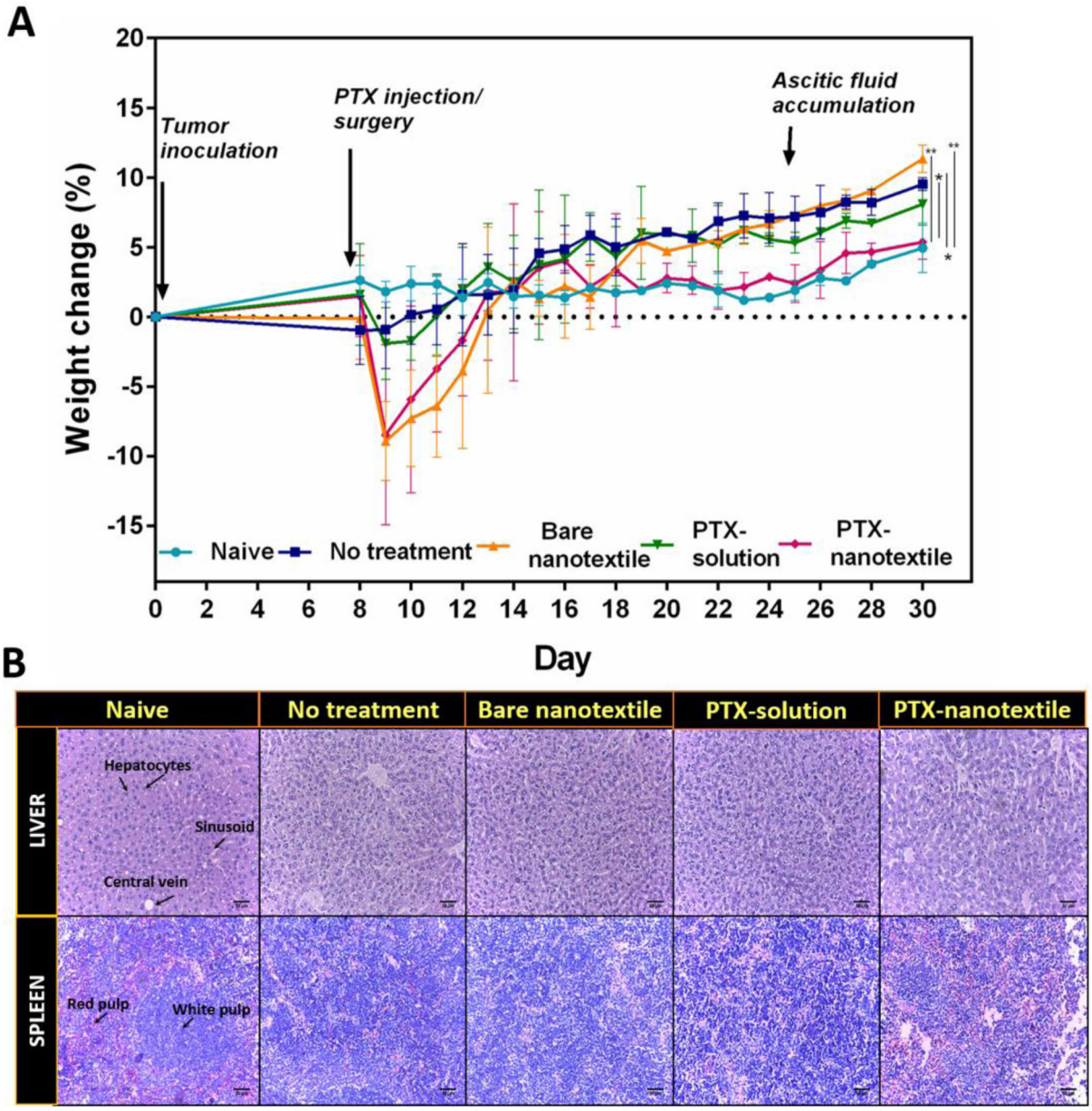


**Figure 6. Body weight changes and histological evaluation of liver and spleen tissues.**

**(A)**The animal body weight changes as a function of time. Data shown are mean±S.D. n =5 and *p < 0.05. **(B)** Histological (H&E stained) images of liver and spleen tissues at day 35 for the control and treatment groups. Scale bar = 50 μm.